Lab on a Chip

RSC Publishing

PAPER

View Article Online
View Journal | View Issue

Rapid dielectrophoretic characterization of single cells using the dielectrophoretic spring†

Cite this: *Lab Chip*, 2013, **13**, 4109

Hao-Wei Su, Javier L. Prieto and Joel Voldman*

Received 27th March 2013,
Accepted 6th August 2013

DOI: 10.1039/c3lc50392e

www.rsc.org/loc

Dielectrophoresis-based cell separation has significant promise for separation of cells from heterogeneous mixtures based on their electrical properties and is used in diverse areas ranging from hematopoietic stem cell purification to cancer cell isolation. The electrical properties of cells in heterogeneous populations determine if and how well cell subpopulations are separable, and therefore the utility of dielectrophoretic separation is fundamentally determined by our ability to measure electrical properties of cell populations on a cell-by-cell basis. We developed an automated system for electrical characterization of cells that can characterize 1000's of individual cells across a range of conditions (>30 conditions/h). The system uses a continuous-flow microfluidic device and a method termed the dielectrophoretic spring that uses the force balance between dielectrophoresis and fluid drag to measure electrical properties of cells independent of size. We present characterization of the method with beads and cells as well as its application to rapidly find conditions that can discriminate neutrophils with different activation states.

Introduction

Cell separations based on intrinsic physical properties allow isolation of cell subpopulations when molecular biomarkers do not exist or are not appropriate.[1] For example, real-time phenotyping cannot afford the sample preparation times common in label-based assays,[2] while surface markers are not always known for immunophenotyping of cells for clinical transplantation.[3,4] Intrinsic physical properties of cells include size, shape, deformability, density, electrical properties, optical properties, *etc*. Electrical properties of cells in particular are of significant interest, and have been correlated to differentiation state of neural stem cells[5] and human embryonic stem cells.[6] Electrical properties are often the basis for cell separation using dielectrophoresis (DEP). DEP has been used in many incarnations for a variety of separations, including different leukocyte subpopulations,[3] viable/non-viable yeast,[4] genetically modified/unmodified bacteria,[7] enrichment of CD34+ cells from peripheral blood stem cell harvests,[8] cancer cells from blood,[2] and isolation of malaria-infected red blood cells.[9] Despite these promising applications, the wider applicability of new DEP separations is constrained by the difficulty in determining whether and under what conditions two cell populations have differing electrical responses and are thus separable. The ideal characterization system would be automated and measure property distributions of a population on a per-cell basis across a range of conditions.

The most common method to characterize the electrical properties of cells is the cross-over frequency (COF) method,[6] which takes advantage of the fact that the DEP response of cells depends on the applied frequency and the suspending medium conductivity. In this method, cells are resuspended in isotonic low-conductivity buffer. By sweeping the frequency and finding the change in response from positive DEP (cells move down the electric-field gradient) to negative DEP (cells move up the electric-field gradient), one can determine the COF of the population. This method, however, typically only provides population-level information (the average COF of the population) and not the per cell distribution, and cannot be applied to measure the properties in a high conductivity medium such as blood plasma or cell-culture media where cells only experience negative DEP and thus do not have a COF.

Other methods exist to measure the electrical properties of cells, including dielectrophoresis-field-flow fractionation (DEP-FFF),[10] Stokes method,[11] iso-dielectric separation,[12] single-cell impedance spectroscopy,[13] optical absorption in microwells with DEP,[14] and electrorotation.[15] However, these can't measure populations on a per-cell basis, with good specificity to electrical properties (and not to other factors such as size, density, *etc.*), while working in native media.

Here we describe a new method and an automated system to measure the electrical properties of cells in different frequencies and different medium conductivity. The method is automated, applied under a continuous flow and measures single-cells at a sufficient throughput to measure the

Department of Electrical Engineering and Computer Science, Massachusetts Institute of Technology, 77 Massachusetts Avenue, Room 36-824, Cambridge, MA 02139, USA. E-mail: voldman@mit.edu; Fax: +1 617-258-5846; Tel: +1 617-253-1583

† Electronic supplementary information (ESI) available. See DOI: 10.1039/c3lc50392e

distribution of a population across many conditions in ~1 h. Furthermore it can determine the electrical properties of cells even in conditions where there is no cross-over frequency such as in native media.

The method is named the DEP spring, and it works by examining the force balance between the spring-like DEP force and fluid drag forces. Because fluid drag can be accurately calculated, we can infer the DEP force, and because the system also measures cell size, we can extract the electrical properties. Here we demonstrate and validate the method, and use it to determine, in ~1 h with >10 000 cells, the electrical characterization and separability of primary human neutrophils.

Results

DEP spring model

The DEP spring method consists of using a force-balance model to measure the DEP forces acting on cells and inferring the electrical properties of individual cells in a continuous manner. Cells enter the microfluidic channel and encounter a negative DEP force (F_{DEP}) that forms a barrier, deflecting the cells (Fig. 1a). A deflected cell reaches a force balance between the hydrodynamic drag (F_{Drag}) and DEP forces and moves along the electrodes. We use δ, the *balance position* between the hydrodynamic force and the DEP force in the direction perpendicular to the electrodes, to extract the electrical properties of the particles.

The relevant forces acting on the deflected cell are predominantly the DEP force and the hydrodynamic (HD) drag force.

HD drag force. For a spherical cell moving in a uniform Stokes' flow (Reynolds number $\ll 1$), the hydrodynamic drag force in the x-direction (F_{Drag}) is given by

$$F_{Drag} = -6\pi R\eta C_{Wall} v_x \quad (1)$$

where R is the radius of the cell, η is the viscosity of the fluid, C_{Wall} is the correction factor that considers the wall effect,[16] and v_x is the average x-velocity of the flow at the center of the cell, given by

$$v_x = \frac{6Q\sin\theta}{wh^3} R(h-R) \quad (2)$$

where Q refers to the volumetric flow rate, w is the channel width, and h is the channel height. This flow rate is evaluated at $z = h - R$ to reflect the fact that the z-directed DEP force is larger than the lift and gravitational forces, pushing the cell to the ceiling of the channel.

DEP force. The analytical representation of the x-directed DEP force (F_{DEPx}) is derived similar to the approach used in DEP-FFF,[10] which is

$$\begin{aligned} F_{DEPx} &= 2\pi R^3 \varepsilon_m \mathrm{Re}[CM] \frac{\partial E^2(x,h-R)}{\partial x} \\ &= 2\pi R^3 \varepsilon_m \mathrm{Re}[CM] q_R(x) V_{RMS}^2 p(f,\sigma_m) \end{aligned} \quad (3)$$

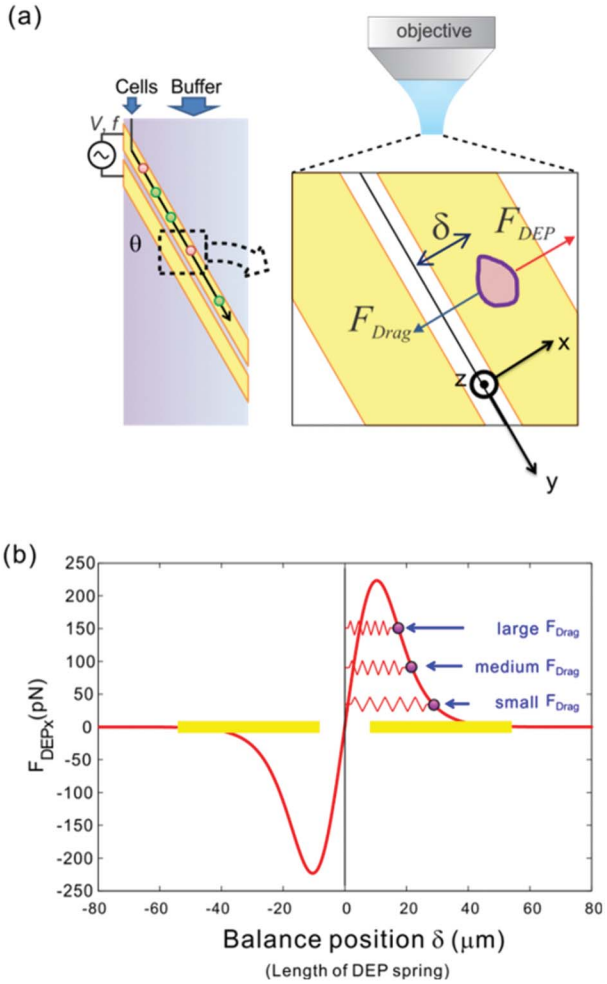

Fig. 1 (a) The DEP spring method overview. Cells (or other particles) are introduced into the channel along with buffer flow. As the cells flow down the channel they encounter the electrodes where they experience a DEP force (red, inset) that balances the drag force (blue, inset). The equilibrium balance position between the two forces is denoted by δ. (b) The DEP force in the x-direction at different balance positions. The balance position decreases when the applied drag force increases, which represents the length of this nonlinear DEP spring. The DEP spring only holds when the drag force is smaller than the maximum DEP force.

where ε_m is the permittivity of the medium and Re[CM] is the real part of the Clausius–Mossotti factor, which encapsulates the electrical properties of the particle. $E^2(x,h-R)$ is the RMS value of the electric field strength modeled from conformal mapping[17] for an applied RMS voltage V_{RMS} at location x and height $h - R$. $p(f,\sigma_m)$ is a normalization factor that corrects for any voltage drop at the electrode/solution interface, and varies with frequency (f) and media conductivity (σ_m). $q_R(x)$ is a function that reflects the positional dependency of the DEP force, which depends on the electrode geometry: the electrode gap (g), the electrode width/spacing (W) and the channel height (h). The detailed analytical expression for $q_R(x)$ is in the ESI† (eqn (S1)).

Balance position. Balancing the two forces gives

$$\overrightarrow{F_{\mathrm{DEP}x}} + \overrightarrow{F_{\mathrm{Drag}}} = 0 \tag{4}$$

We define this *balance position* as δ which is the length of the nonlinear DEP spring.

$$\delta = {q_{\mathrm{R}}}^{-1}\left(\frac{3C_{\mathrm{Wall}}\eta\sin\theta\left[\frac{6Q}{wh^3}(h-R)\right]}{R\varepsilon_{\mathrm{m}}\mathrm{Re[CM]}{V_{\mathrm{RMS}}}^2 p(f,\sigma_{\mathrm{m}})}\right) \tag{5}$$

The balance position decreases with the applied HD drag force, and increases with the voltage or Re[CM] (Fig. 1b). If the HD drag force surpasses the maximum DEP force, the spring will break down and the cell will pass through the barrier.

Inferring the real part of the Clausius–Mossotti factor Re[CM]. Re[CM], which contains the electrical properties of the particle, can be extracted from δ by inverting the expression, resulting in

$$\begin{aligned}\mathrm{Re[CM]} &= \left[\frac{18Q\eta\sin\theta}{{V_{\mathrm{RMS}}}^2 wh^3\varepsilon_{\mathrm{m}}p(f,\sigma_{\mathrm{m}})}\right]\left[\frac{C_{\mathrm{Wall}}(h-R)}{Rq_{\mathrm{R}}(\delta)}\right] = \beta\gamma \\ \beta &= \frac{18Q\eta\sin\theta}{{V_{\mathrm{RMS}}}^2 wh^3\varepsilon_{\mathrm{m}}p(f,\sigma_{\mathrm{m}})} \\ \gamma &= \frac{C_{\mathrm{Wall}}(h-R)}{Rq_{\mathrm{R}}(\delta)}\end{aligned} \tag{6}$$

Re[CM] is thus a product of two terms: β which is system-dependent but particle independent, and γ, which represents the particle properties. Thus, determining Re[CM] requires simultaneous measurement of size (R) and δ and either measurement/knowledge of the other unknown parameters (ε_{m}, η, $p(f, \sigma_{\mathrm{m}})$, *etc.*) or calibration of β using standardized particles with known R and Re[CM].

Automated measurement system

Efficient measurement of the electrical properties of many cells requires an automated system to sweep across different parameters and record data on a cell-by-cell basis. In particular, DEP forces (and in turn, electrical properties) depend on the applied frequency (f) and the media conductivity (σ_{m}). However, changing these conditions manually, especially the media conductivity which requires centrifuging steps that are time-consuming, makes systematic measurement tedious. Most importantly, since the electrical properties of some cell types are time-sensitive, such as neutrophil activation levels,[18] cells undergoing apoptosis,[19] *etc.*, it is important to minimize characterization time. Therefore, we developed an automated system for cell characterization with a throughput of thousands of cells h^{-1} ($\sim$10 cells s^{-1}), which is sufficient for characterizing enough cells to determine the population distributions of electrical properties at different frequencies and media conductivities.

The system (Fig. 2a) uses a computer-controlled function generator (for electrical stimulation), syringe pumps, microscope, and algorithms to completely automate population characterization. We use two different approaches for changing the media conductivity: (i) changing conductivity over time by creating a uniform conductivity in the channel that we can vary with time, or (ii) changing conductivity in space, by having a gradient of conductivity in the channel that the cells pass through, where by changing the measurement position we effectively change the conductivity at which the cells are being measured. For the first approach (Fig. 2b), we use off-chip mixing of high conductivity media (PBS) and low

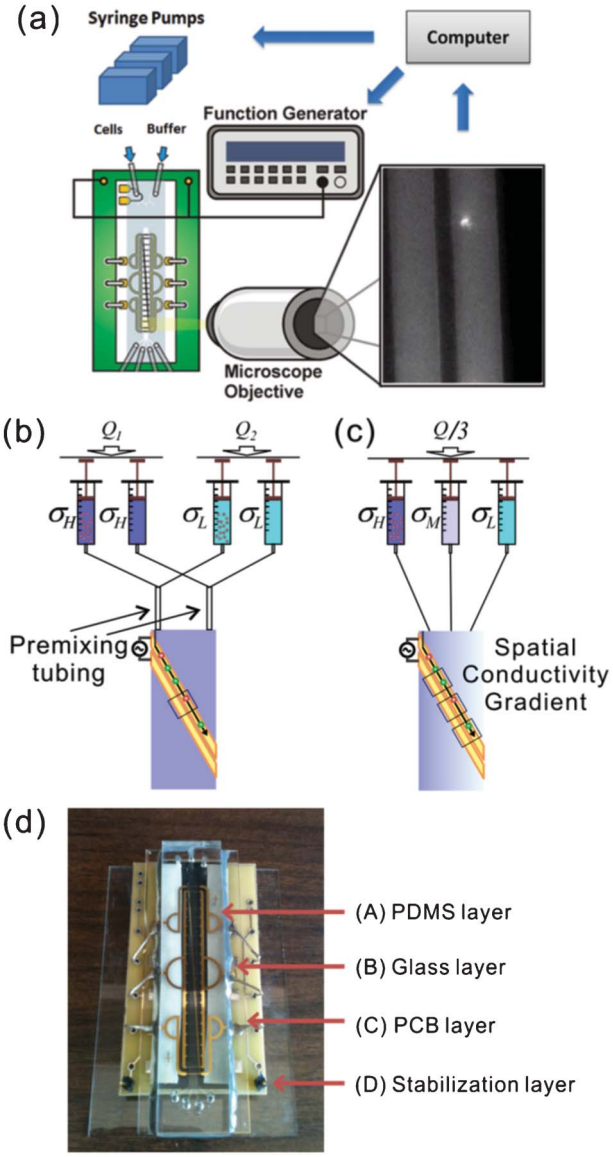

Fig. 2 (a) Schematic of automated system for changing frequencies and media conductivities and controlling the microscope and camera for data acquisition. (b) Changing the media conductivity in time by adjusting the flow rate ratio of high(σ_H)/low(σ_L) conductivity media to dynamically control the media conductivity and the overall flow rate ($Q = Q_1 + Q_2$). (c) Changing the media conductivity in space by generating a conductivity gradient and imaging at different field of views. (d) Image of fabricated microfluidic device, showing the device (PDMS and glass layers), underlying printed-circuit board (PCB), and PDMS stabilization layer.

conductivity media (isotonic sucrose-dextrose solution) with different flow rates, which creates a known uniform conductivity intermediate between the two extremes. Similar to Lin *et al.*,[20] we control the flow rates of two syringe pumps to enable independent control over media conductivity and overall flow rate Q. Void volumes are minimized to keep lag times to ~1 min between changes in conductivity. For the second approach (Fig. 2c), we generate a conductivity gradient on-chip using three syringes of differing conductivities and allowing for transverse diffusion, using previously validated models[12] to infer the local conductivity at various parts of the channel. We used the time-varying conductivity for the HL-60 cells' characterization, and the spatially-varying conductivity with the neutrophils.

We use a fully automated microscope with camera to acquire images, and MATLAB-based software that both controls the overall system and processes the images to find cells, measure R, and measure δ. The resulting system is able to acquire ~250 000 cell images over ~1 h, from which ~20 000 different cells are typically identified, post-processed, and analyzed.

Model validation with polystyrene beads

We used well-defined test particles to quantitatively validate the DEP spring model (eqn (5)) using a microfabricated angled-electrode device (Fig. 2d) with h = 17 μm and W = 46 μm. We measured the balance positions of polystyrene beads across different flow rates and voltages (~200 beads/condition) at a frequency of 1 MHz and media conductivity of 20 mS m^{-1}. Polystyrene beads are provided with a known size, and because polystyrene is nonconducting and the beads are too large for surface conductance to be important, they have an expected Re[CM] = −0.49 at the frequency and media conductivity used here, similar to what others have seen.[17] For these particles we find that, as expected, the balance position increases with increasing voltage (Fig. 3a) and decreases with increasing flow rate Q (Fig. 3b).

The measured balance positions are approximately normally distributed (mean: 41.9 μm, st. dev. 1.2 μm) (Fig. 3c). The width of the distribution is due to a combination of variations in particle size and imprecision in the balance position measurement. Assuming that the particle size is normally distributed with a manufacturer-specified 10% C.V. (verified with Coulter Counter), and linearizing the balance position model to determine its size sensitivity, gives a deviation of ± 0.7 μm to δ due to size variation. Thus, the imprecision due to the measurement contributes ~± 0.96 μm assuming that these contributions are also normally distributed and independent of the particle size. These remaining variation likely arises from the segmentation process (pixel size is 1.07 μm) and temporal variation in the flow rates and electrical field intensity.

Examining the quantitative trends in δ across voltage and flow rate (Fig. 3d), we find that at as expected, the balance position decreases with increasing flow rate because the DEP spring is being increasingly compressed with higher HD drag force. For a given flow rate, if we increase the voltage, the balance position also increases because the increased voltage increases the n-DEP force, which makes the DEP spring stiffer.

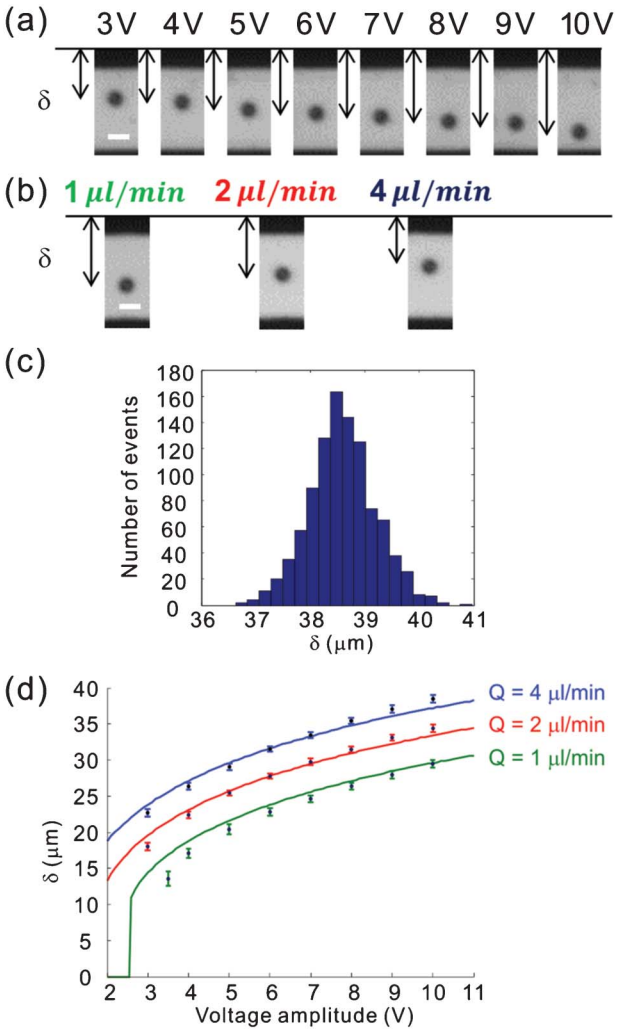

Fig. 3 Validation of DEP spring model. (a) Representative images of particles (median balance position) at different voltages (Q = 1 μl min^{-1}). The scale bar is 10 μm. (b) Representative images of particles (median balance position) at different flow rates (V = 7 V). The scale bar is 10 μm. (c) Representative balance position histogram (Q = 4 μL min^{-1} and V = 7 V). (d) Measured (○, mean ±1 std. dev.) and calculated (—) balance positions across different Q and V (n ~ 200 particles/condition).

If we predict the balance position *via* direct calculation from known and measured parameters (ESI† Table S1), we find an average deviation between theory and experiment of 4% without any fitting parameters. If we fit all the data to determine the best overall system parameter, β we find that the fitted β matches the direct calculation of β to within 8%. For balance positions near the electrode edge, the deviation between the model and experimental results increases (maximum deviation ~20% for V = 3.5 V and Q = 4 μL min^{-1}), which implies the existence of secondary forces. Constant frictional forces are unlikely to explain the deviations, since those should be independent of the balance position. Electrohydrodynamics forces are one potential cause. However, for balance positions in the range of 20 μm–40 μm, which is where the proceeding experiments are per-

formed, our model agrees well with experiments and thus adequately captures the relevant.

Rapid characterization of HL-60 cells in multiple conditions

We chose the human leukemia HL-60 cell line as our first target for electrical cell characterization. HL-60s have been electrically characterized previously[10,21] but only the mean electrical properties were reported, and due to limitations of the techniques the cells were only measured in low media conductivities. Electrical properties of cells are known to depend on the media conductivity,[22–24] so these prior characterizations did not provide a full view of the cells' electrical properties. We used the DEP spring to infer Re[CM] of HL-60s (eqn (6)), measuring >10 000 cells across 5 media conductivities and 8 frequencies in ~1 h in an automated fashion. For these experiments we used spatially uniform media conductivity (Fig. 2b).

We first verified the ability to optically measure the sizes of the cells. Using background correction and thresholding of the bright field image (5% of the electrode brightness) (ESI† Fig. S1a), we found that the optically measured size distribution of HL-60s (mean 12.23 μm, st. dev. 2.00 μm) was well matched to the distribution obtained *via* Coulter sizing (mean 11.77 μm, st. dev. 1.99 μm) (ESI† Fig. S1b), and was independent of the focal plane (2.5% variation in the distribution mean across ±10 μm change focus position) when using a low-numerical-aperture objective (10×, N.A. 0.25).

Since the electrical properties of cells are more complicated than those of beads, they require measurement across both frequency and solution conductivity, which will result in variations in the system-dependent factor $p(f, \sigma_m)$, that accounts for the frequency- and conductivity-dependent voltage drop at the electrode/solution interface. Therefore, we incorporated 6 and 10 μm beads along with the cells as references to calibrate the systematic parameter (β). We used imaging algorithms to automatically find and classify images of beads and cells as they flowed along the electrodes (ESI† Fig. S1c) so that we can measure the balance positions of them together and implement real-time calibration. The algorithm had an accuracy of 96% as compared to manual classification of 3000 particle images. The 4% inaccuracy primarily affected the 10 μm beads, causing the 10 μm bead histogram to deviate from a Gaussian distribution.

To analyze the data, first we compared the balance position histogram of beads and cells across frequency (Fig. 4a). For the beads, the balance positions do not change appreciably across >100-fold variation in frequency (4% variation in the mean for 6 μm beads and 6% variation for 10 μm beads, from 0.1 MHz to 12.8 MHz). This is because the frequency response of the system $p(f, \sigma_m)$ is approximately flat (as measured by impedance analyser, ESI† Fig. S2) and the Re[CM] of the beads is ~−0.5 (ESI† Fig. S3) across these frequencies.

At 0.1 MHz, the cells' balance position was similar to that of the 10 μm beads (Fig. 4a). Because the cells are similar in size to the 10 μm beads, the similarity in δ implies that Re[CM] for the cells should be close to that of beads. This makes sense because the cells' effective conductivity is much smaller than the surrounding media at this frequency and so the cells act as

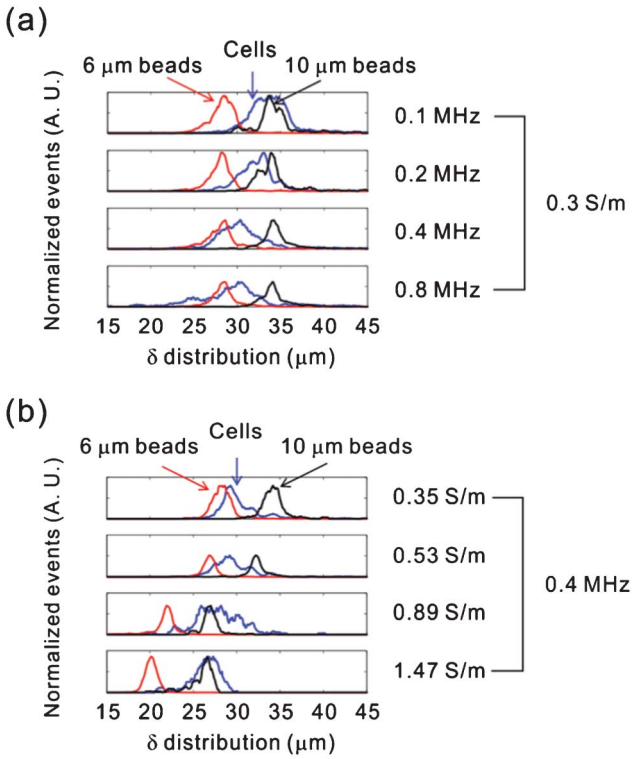

Fig. 4 Measured balance position histograms of the HL-60 cells (blue), 6 μm beads (red), and 10 μm beads (black) in (a) 0.3 S m^{-1} media at different frequencies, and (b) at 0.4 MHz and different media conductivities.

insulating spheres, making their DEP response similar to the non-conducting beads.

At higher frequencies, the cell population shifts to smaller δ. This shift is to be expected from the electrical model of cells, because at higher frequencies the electric field penetrates the plasma membrane, and the electrical properties are dependent on the cytoplasmic conductivity, resulting in a smaller magnitude for Re[CM]. We also observe that the width of the distribution increases at 0.4 MHz and 0.8 MHz as compared to 0.1 MHz. This qualitatively suggests that the Re[CM] of individual cells moves away from ~−0.5 in different degrees, reflecting increased heterogeneity of the electrical properties of cells within the population. Acquiring such information about population heterogeneity is one of the strengths of high-throughput single-cell methods such as the DEP spring.

For frequencies greater than 0.8 MHz, some of the cells' Re[CM] decreases enough that the drag force exceeds the n-DEP force and the cells pass through the electrodes. In other words, there is a minimum Re[CM] that can be measured, which depends on the flow rate and voltage used, and can also be changed by changing the device geometry. For the conditions used here, we can estimate the minimum Re[CM] that can be measured for ~10 μm cells ranges from −0.087 (for 1.47 S m^{-1}) to −0.022 (for 0.3 S m^{-1}). If desired, the minimum measurable Re[CM] can be decreased further by decreasing flow rate, with a commensurate decrease in throughput.

We next compare the balance position histograms across media conductivities (Fig. 4b). We see that the balance positions of the beads decrease with increasing conductivity, consistent with the fact that the voltage drop in the liquid is reduced when the impedance of the liquid decreases and becomes comparable with the 50 Ω output resistance of the function generator. At the highest conductivity (1.47 S m^{-1}), the balance positions of the cells are similar to that of the 10 μm beads. Because the two populations have similar mean sizes, this implies that the cells' Re[CM] is near −0.5, which is supported by electrical models of cells, which at these frequencies have an effective conductivity that is much smaller than that of the surrounding media. At the lowest conductivity (0.35 S m^{-1}), the balance positions of the cells are more similar to that of the 6 μm beads, implying a decrease in cells' Re[CM] to ∼−0.25, which is consistent with a decreased contrast in media conductivity *versus* cell effective conductivity when the media conductivity decreases.

The above discussion qualitatively illustrates how one can use the known properties (R, Re[CM]) of the beads to infer the Re[CM] of cells in the presence of variations in $p(f, \sigma_m)$. Quantitatively extending this approach, we used the 6 μm bead locations to infer β at different frequencies and conductivities. Then, using the measured R and δ for individual cells, we were able to infer, for the first time, Re[CM] for thousands of single cells across 39 different frequency and conductivity combinations. This provides Re[CM] distributions at each measurement condition (Fig. 5).

We compared the Re[CM] distributions with the values predicted from a single-shell model (blue lines in Fig. 5) using measurements of HL-60s at low media conductivities(56 mS m^{-1}).[10] We find that our measurements of Re[CM] agree with the general trend of the single-shell model, namely that the Re[CM] is near −0.5 at low frequency and high media conductivity and moves closer to zero when the frequency increases or the conductivity decreases. Quantitatively, for cases where the single-shell model gave Re[CM] < −0.2 (distributions without gray color), the mean of the experimental Re[CM] distribution matches the model to within 0.12 (24%).

For cells below the expected minimal measurable Re[CM] for each condition, the HD drag force will overcome the repulsive DEP force and cells will not be measured, biasing the measurements. Interestingly, even under conditions where the model-predicted Re[CM] is substantially positive (and thus the cells experience p-DEP), we find that a significant fraction of cells experience n-DEP and are measured in our system (0.3 S m^{-1} and >1 MHz), again emphasizing that average Re[CM] values do not represent the complexity found in a given cell population.

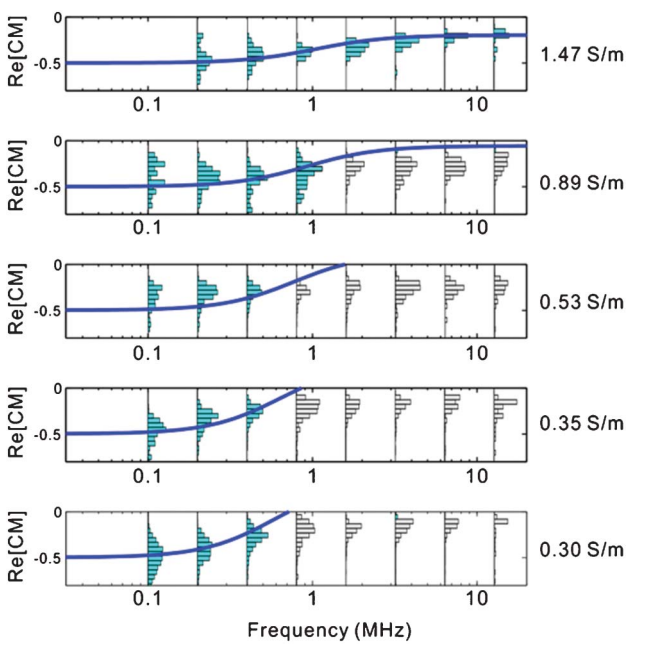

Fig. 5 Extracted Re[CM] histograms at different frequencies and conductivities, compared to predicted Re[CM] (blue line) from a single-shell model.[10] The distributions where the model-predicted Re[CM] > −0.2 (gray color) are regions where part of the cell population would experience positive DEP.

Discrimination of activated and unactivated neutrophils using DEP spring

Neutrophil activation plays an important role in the immunopathogenesis of a range of diseases,[25,26] and thus electrically measuring neutrophil activation and/or separating activated neutrophils has applications across basic biology and medicine. However, electrical assessment of activation requires finding conditions that can distinguish activated from unactivated populations. A further challenge is that neutrophils are easily activated due to exposure to non-physiological media, and thus experimental conditions need to be innocuous and measurement time needs to be minimized. Here we used the DEP spring to automatically measure the electrical properties of activated and unactivated neutrophils across 7 different frequencies and 3 media conductivities in order to identify conditions where they could be distinguished. We used the spatial conductivity gradient method (Fig. 2c) for these experiments to minimize the time the cells were exposed to low conductivity media (∼s). The positive control of activated neutrophils was activated with 1 μM PMA for 20 min at room temperature, resulting in an activation percentage of 93.9% (ESI† Fig. S4). During the ∼1 min measurement time for of each condition in our system, the balance positions were temporally stable.

We plot the measured balance positions of the cells in Fig. 6. In high-conductivity medium (1.36 S m^{-1}), both activated and unactivated cells have similar balance positions at all frequencies. We also see a peak in the histogram at small balance position, which is due to contaminating erythrocytes remaining from the sample prep. For the middle conductivity (0.89 S m^{-1}), however, the balance positions of the activated neutrophils decrease more than that of the unactivated cells as the frequency increases. At low media conductivity, the cell number decreases when the frequency increases because the cells' start to experience pDEP and are not retained by the barrier. From this data it is apparent that the two cells populations are distinguishable, and further that middle conductivity (0.89 S m^{-1}) and high frequency (⩾6.4 MHz) give the best discernment, with an area-under-the-curve of the

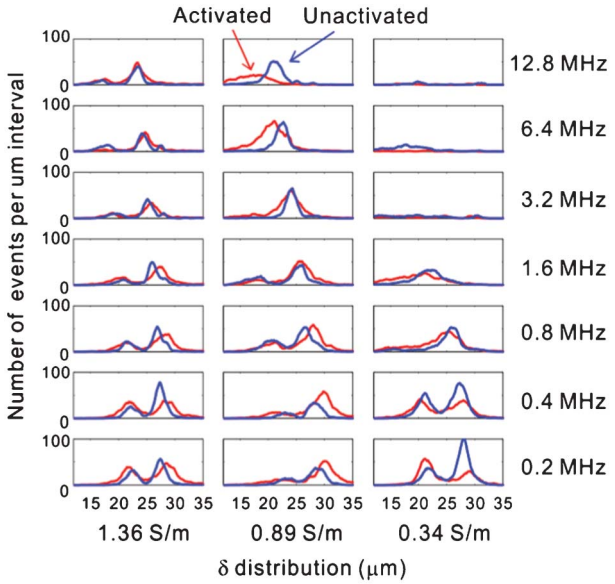

Fig. 6 The balance position histograms of activated (red) and unactivated (blue) neutrophils at different frequencies and conductivities.

receiver-operator characteristic of 0.78. This ability to quickly measure entire population distributions across different conditions is one of the defining features of the DEP spring method.

Discussion

We have developed a new method for measuring electrical properties of cells. The key features of the DEP spring are that it is continuous, captures size information, is fast enough to measure populations on a cell-by-cell basis, and is automated to allow searching across different operating regimes. Because the method captures size information and uses microscopy, Re[CM] can be extracted from the DEP and hydrodynamic drag force balance. We verified the method with beads, and showed results with HL-60 cells and use the DEP spring to determine the separation conditions for activated and non-activated neutrophils.

The DEP spring is an important addition to the cohort of methods to electrically characterize cells. Single-cell impedance measurement methods also provide Re[CM] with high throughput,[13,27] but do not typically operate in cells' natural (high-conductivity) media, and cells' properties have been shown to be media conductivity-dependent.[22–24] More importantly, impedance cytometry is most powerfully applied in a flow cytometric approach, where the goal is to distinguish populations of cells rather than to infer their underlying absolute properties. Thus, we are not aware of any work with impedance cytometry that extracts out the underlying electrical properties, making it difficult to generalize measurements across systems, though such an effort to make absolute measurements would be welcome.

DEP-FFF,[10] meanwhile, is also dependent on cell density. Among methods that can image, electrorotation[15] also provides information closely related to Re[CM], and has been automated,[28] but it is tedious to measure cells across multiple medium conditions. The Stokes method[11] and other related velocity-measurement methods[29] require particle tracking, whereas the DEP spring only requires one image to make the measurement.

The ability to extract distributions of Re[CM] is important because it is applicable across all DEP device architectures; one can design a custom device for separating any two particular cell populations once their Re[CM] and R distributions are defined, because the DEP force on those particles can be re-calculated under different conditions.

Re[CM] compares the complex polarizability of the cell and media.[30] The ability to extract out the Re[CM] distributions of cells at different frequencies and media conductivities provides insight into the heterogeneity of the electrical properties of the cells. This is critical to evaluating the utility of proposed DEP separation methods, because the separability of populations depends not only on the differences of their means but the width of the distributions. Because the DEP spring makes it straightforward to accumulate single-cell Re[CM] data, one can develop more nuanced electrical cell models that better represent the DEP behavior of a cell population.

Finally, we note that the balance positions provide fundamental information about the electrical separability of cells in the device (angled coplanar electrodes). The balance positions of cells reflect the margin of the DEP barrier *versus* the HD flow (*i.e.*, the ratio between the maximum DEP force and the current drag force). Therefore, any observed difference in balance positions indicates that two cell populations are separable on the device simply by increasing the flow rate (*i.e.*, cells with smaller balance positions will pass through the barrier at a lower flow rate than cells with a larger balance position). Thus, although it is likely preferable to design specialized devices for electrical cell separation once the electrical properties of any two populations are known, it is also possible to use the balance position information to directly carry out a separation in the current device.

Conclusions

We developed a novel method and an automated system for rapid DEP characterization. We demonstrate the first high-throughput DEP single-cell characterization of different frequencies and conductivities (including high conductivity media). We used this method to find conditions under which activated and unactivated neutrophils have different DEP responses and thus are electrically separable. The system can accumulate large datasets for different cell types for electrical studies of cells and applications of label-free DEP separation.

Compared to other existing methods, the ability to extract out the Re[CM] distributions of cells at different frequencies

and media conductivities provides insight into the heterogeneity of the electrical properties of the cells. This is critical to evaluating the utility of proposed DEP separation methods, because the separability of populations depends not only on the differences of their means but the width of the distributions. Because the DEP spring makes it straightforward to accumulate single-cell Re[CM] data, one can develop more nuanced electrical cell models that better represent the DEP behavior of a cell population using our single-cell datasets.

Materials and methods

Reagents

We used 6 μm (6.081 ± 0.195 μm) and 10 μm (10.269 ± 0.502 μm) carboxyl-modified polystyrene beads (Polyscience) for model validation and calibration. The HL-60 cell lines were cultured in media (DMEM/20% FBS/1× Penstrip) in T75 flasks, and used 24 h after seeding.

Automated system

A computer-controlled function generator (Agilent 33 250 A) was connected to the microfluidic device *via* 50 Ω co-axial cable with BNC connectors. Flow was delivered by computer-controlled syringe pumps (Chemyx Fusion 200) using syringes (Hamilton 1 mL Gastight Syringes) connected to the device *via* 0.004 I.D. PEEK™ tubing (IDEX Health and Science). Imaging was performed on a fully automated upright microscope (Zeiss Axio Imager.m1m) with stage control (MAC 5000), both interfaced through the Zeiss MTB2012 server and ImageJ core and controlled by MATLAB. Images were acquired by a PCO Sensicam QE camera also controlled *via* MATLAB.

Microfluidic device

The device (Fig. 2d) consists of four layers: (A) 5–7 mm thick PDMS layer which includes a microfluidic channel (20 μm by 2 mm by 5 cm) molded from an SU-8-on–silicon mold or a plastic master mold replicated from the original mold.[31] We punched holes in the PDMS layer and cleaned the surface with Scotch tape before plasma bounding. (B) A 762-μm thick Pyrex wafer with Au/Ti (200 nm/10 nm) electrodes patterned using a conventional lift-off process (negative resist NR-7). This layer is plasma-bonded to layer (A), followed by baking (80 °C for 30 min). For additional robustness, we sealed the side of the two layers with two-part epoxy (3M Scotch-Weld™ 2216 B/A). (C) A printed circuit board (PCB) interface board to connect between the chip electrodes and external connections. We used conductive epoxy to connect the electrode and the printed circuit board. (D) A bottom layer of PDMS (~5 mm thick) used to stabilize the chip on the microscope stage.

Frequency response measurement

We characterized the frequency response of the electrodes using an impedance analyzer (Agilent 4294A).

Image analysis

The recorded videos were processed *via* MATLAB frame by frame. Background images were obtained through a time-domain median filter. We calculated the difference between the raw images and background and transformed the images into binary images with a threshold of 0.05, which resulted in accurate cell size measurements as compared to Coulter Counter (ESI† Fig. S1b). We identified the cell objects in the binary images and extracted out their morphometric properties: area, balance positions, intensity, *etc*.

HL-60 preparation

We centrifuged the cells and resuspended them into isotonic high-conductivity media (1× PBS/0.75% BSA/1 mM EDTA) and low conductivity media (8.5% Sucrose/0.3% Dextrose/0.75% BSA). The conductivity of the liquid was measured with a commercial conductivity meter (Thermo Orion pHuture™ Meter, Model 555A) at room temperature.

Neutrophil isolation and activation

Fresh heparinated human blood was obtained from healthy human donors (Blood Research Components) the day of the experiments. 5 ml of whole blood was carefully layered on top of 3 ml of Mono-Poly Resolving Medium (MP Biomedicals) and centrifuged at 400 g for 40 min. After centrifugation, neutrophils were recovered from the second fraction of the density column. Neutrophils were washed and resuspended in 0.5 ml of 1× PBS/0.75% BSA and 1U heparin. A solution of 2 μM PMA was prepared in 1× PBS with calcium and magnesium/0.75% BSA and 1U heparin. Half the neutrophils were activated by mixing them 1 : 1 with the PMA solution achieving a final concentration of 1 μM PMA and incubating 20 min at room temperature. The other half was mixed 1 : 1 with the vehicle fluid (in 1× PBS with calcium and magnesium/0.75% BSA and 1U heparin) and was used as unactivated control. Both activated and unactivated cells were centrifuged at 200 g for 5 min and resuspended in the high-conductivity media (1× PBS/0.75% BSA/1U heparin). Low-conductivity media (8.5% Sucrose/0.3% Dextrose/0.75% BSA) and middle-conductivity media buffer (1 : 1 ratio of high and low conductivity media buffer) were used to create the spatial conductivity gradient. For validation of activation, we took a portion of both activated and unactivated cells and stained with PE-conjugated mouse anti-human CD66b monoclonal antibody (BD Biosciences, Accuri) and APC-conjugated mouse anti-human CD18 monoclonal antibody for 30 min in the dark at 4 °C. After staining, we washed the sample with buffer and analyzed them with flow cytometry (BD Biosciences, Accuri C6). The activation percentage (CD18+) was 94% for PMA-treated neutrophils (CD66b+) *versus* 0.25% for untreated cells (ESI† Fig. S4).

Acknowledgements

This work is funded in part by the National Science Foundation (DBI-0852654) and DARPA *via* the Space and Naval Warfare Systems Center (N66001-11-1-4182). We thank the Microsystems Technology Laboratory for fabrication assistance.

References

1 D. R. Gossett, W. M. Weaver, A. J. Mach, S. C. Hur, H. T. K. Tse, W. Lee, H. Amini and D. Di Carlo, *Anal. Bioanal. Chem.*, 2010, **397**, 3249–67.
2 P. R. C. Gascoyne, X.-B. Wang, Y. Huang and F. F. Becker, *IEEE Trans. Ind. Appl.*, 1997, **33**, 670–678.
3 J. Yang, Y. Huang, X. B. Wang, F. F. Becker and P. R. Gascoyne, *Biophys. J.*, 2000, **78**, 2680–9.
4 G. H. Markx, M. S. Talary and R. Pethig, *J. Biotechnol.*, 1994, **32**, 29–37.
5 L. A. Flanagan, J. Lu, L. Wang, S. A. Marchenko, N. L. Jeon, A. P. Lee and E. S. Monuki, *Stem Cells*, 2008, **26**, 656–65.
6 S. Velugotla, S. Pells, H. K. Mjoseng, C. R. E. Duffy, S. Smith, P. De Sousa and R. Pethig, *Biomicrofluidics*, 2012, **6**, 044113.
7 M. Castellarnau, A. Errachid, C. Madrid, A. Juárez and J. Samitier, *Biophys. J.*, 2006, **91**, 3937–45.
8 M. Stephens, M. S. Talary, R. Pethig, A. K. Burnett and K. I. Mills, *Bone marrow transplantation*, 1996, **18**, 777–82.
9 P. Gascoyne, C. Mahidol, M. Ruchirawat, J. Satayavivad, P. Watcharasit and F. F. Becker, *Lab Chip*, 2002, **2**, 70–5.
10 Y. Huang, X. B. Wang, F. F. Becker and P. R. Gascoyne, *Biophys. J.*, 1997, **73**, 1118–29.
11 J. M. Cruz and F. J. Garcia-Diego, *IAS '97. Conference Record of the 1997 IEEE Industry Applications Conference Thirty-Second IAS Annual Meeting*, 1997, **3**, 2012–2018.
12 M. D. Vahey and J. Voldman, *Anal. Chem.*, 2008, **80**, 3135–43.
13 T. Sun and H. Morgan, *Microfluid. Nanofluid.*, 2010, **8**, 423–443.
14 H. O. Fatoyinbo, K. F. Hoettges and M. P. Hughes, *Electrophoresis*, 2008, **29**, 3–10.
15 R. Hölzel, *Biophys. J.*, 1997, **73**, 1103–9.
16 P. Ganatos, R. Pfeffer and S. Weinbaum, *J. Fluid Mech.*, 1980, **99**, 755.
17 N. Demierre, T. Braschler, P. Linderholm, U. Seger, H. van Lintel and P. Renaud, *Lab Chip*, 2007, **7**, 355–65.
18 I. Perry, S. M. Buttrum and G. B. Nash, *Br. J. Pharmacol.*, 1993, **110**, 1630–1634.
19 C. Huang, A. Chen, M. Guo and J. Yu, *Biotechnol. Lett.*, 2007, **29**, 1307–1313.
20 F. Lin, W. Saadi, S. W. Rhee, S.-J. Wang, S. Mittal and N. L. Jeon, *Lab Chip*, 2004, **4**, 164–7.
21 F. F. Beckert, X.-B. Wang, Y. Huang, R. Pethig, J. Vykoukal and P. R. C. Gascoyne, *J. Phys. D: Appl. Phys.*, 1994, **27**, 2659–2662.
22 M. D. Vahey and J. Voldman, *Anal. Chem.*, 2009, **81**, 2446–55.
23 S. P. Yu, L. M. Canzoniero and D. W. Choi, *Curr. Opin. Cell Biol.*, 2001, **13**, 405–411.
24 B. W. J. D. Alberts, D. Bray, J. Lewis, M. Raff and K. Roberts, *Molecular Biology of the Cell*, Garland Publishing, New York, 3rd edn, 1995.
25 B. Amulic, C. Cazalet, G. L. Hayes, K. D. Metzler and A. Zychlinsky, *Annu. Rev. Immunol.*, 2012, **30**, 459–89.
26 J. Cohen, *Nature*, 2002, **420**, 885–91.
27 K. Cheung, S. Gawad and P. Renaud, *Cytometry, Part A*, 2005, **65**, 124–132.
28 G. De Gasperis, X. B. Wang, J. Yang, F. F. Becker and P. R. C. Gascoyne, *Meas. Sci. Technol.*, 1998, **9**, 518–529.
29 F. Gielen, A. J. Demello and J. B. Edel, *Anal. Chem.*, 2012, **84**, 1849–1853.
30 H. Morgan and N. G. Green, *AC Electrokinetics: Colloids and Nanoparticles*, Research Studies Press, Ltd., 2003.
31 S. P. Desai, D. M. Freeman and J. Voldman, *Lab Chip*, 2009, **9**, 1631–7.